



# A million-year-scale astronomical control on Late Cretaceous sea-level

Jens E. Wendler<sup>1,3,\*</sup>, Stephen R. Meyers<sup>2</sup>, Ines Wendler<sup>1,3</sup>,  
and Jochen Kuss<sup>3</sup>

With 8 figures and 1 table

**Abstract.** An evaluation of the global synchronicity and duration of “3<sup>rd</sup>-order” sea-level fluctuations during the Cretaceous greenhouse has been hampered by poor constraints on potential climatic and tectonic drivers, and limitations of geochronology and chronostratigraphic correlation. To provide insight into the nature of such sea-level fluctuations, here we present a new Late Cretaceous record from the Jordanian Levant Platform, comprising a detailed physical-, bio-, chemo- and sequence stratigraphy. Carbonate content of these strata reflects overall sequence stratigraphic development, and demonstrates a dramatic 3<sup>rd</sup>-order-scale cycle that is also apparent in the  $\delta^{13}\text{C}$  record. Updated radioisotopic constraints and astrochronologic testing provide support for the inference of an ~1 million year long sea-level oscillation associated with this 3<sup>rd</sup>-order cycle, which likely reflects a long-period obliquity (1.2 Myr) control on eustasy and stratigraphic sequence development, linked to the global carbon cycle. The observation of cyclic sea-level fluctuations on this time scale suggests sustained global modulation of continental fresh-water-storage. The hypothesized link between astronomical forcing and sea-level forms a baseline approach in the global correlation of sequence boundaries.

**Key words.** Cyclostratigraphy, Astronomical forcing, Sequence stratigraphy, Time series analysis, Late Cretaceous, Cenomanian/Turonian

## 1. Introduction

Sequence stratigraphy is one of the primary tools for the evaluation of sea-level change throughout Earth history and provides a powerful framework for regional and global correlation on multiple time scales (Haq et al. 1987, Hardenbol et al. 1998, Simmons et al. 2007). However, the global correlation of stratigraphic sequences in the Mesozoic, specifically 3<sup>rd</sup>-order (assigned in the literature to differing time intervals of

~0.5 to 3 Myr) sequences and shorter, has proven problematic for three reasons: (A) limitations of geochronology and chronostratigraphic correlation, (B) differences in sequence stratigraphic approaches and concepts of sequence-orders between locations, and (C) uncertainties regarding the two main drivers of sea-level in platforms, local tectonics and eustasy. Regarding the last point, understanding large Cretaceous eustatic fluctuations is problematic given a presumed ice-free Earth, and alternatively, tectonics may repre-

---

### Authors' addresses:

<sup>1</sup> Smithsonian Institution, NMNH, Department of Paleobiology, P.O. Box 37012, Washington D.C. 20013-7012, USA

<sup>2</sup> University of Wisconsin – Madison, Department of Geoscience, 1215 W. Dayton St., Madison, WI 53706, USA

<sup>3</sup> Bremen University, Geoscience Department, P.O. Box 330440, 28334 Bremen, Germany

\* **Corresponding author:** Mailing address: Bremen University, Geoscience Department, P.O. Box 330440, 28334 Bremen, Germany. E-Mail: wendler@uni-bremen.de

sent the main control on some platform carbonate cyclicity (Bosence et al. 2009). Nonetheless, an increasing number of cyclostratigraphic analyses suggest that Mesozoic 3<sup>rd</sup>-order sequences could represent the 400 kyr eccentricity cycle (Strasser et al. 2000, Gale et al. 2002), as well as longer period cycles such as the ~1.2 Myr obliquity cycle and particularly the ~2.4 Myr eccentricity cycle (Herbert 1999, Matthews and Frohlich 2002, Sprovieri et al. 2006, Kuhnt et al. 2009, Wendler, I. et al. 2009, Wendler et al. 2010, Boulila et al. 2011, Batenburg et al. 2012, Sprovieri et al. 2013). However, the statistical significance and suitability of spectral analytical methods used in such analyses is heterogeneous (e. g., Vaughan et al. 2011, Meyers 2012), and rigorous tests are required, particularly when assessing shallow marine sections that are sensitive to sea level fluctuations. Independent of astronomical forcing studies, onlap surfaces of the six Cenomanian 3<sup>rd</sup>-order sequences of the Anglo-Paris Basin were shown to be spaced by ~1 Myr (Robaszynski et al. 1998). A link between 3<sup>rd</sup>-order sea-level fluctuations and glaciation, as a nonlinear response to the ~1.2 Myr amplitude modulation of obliquity, has also been proposed for Cenozoic sequences (Lourens and Hilgen 1997, Wade and Pälike 2004, Pälike et al. 2006), suggesting that astronomical influence on eustasy may be a common feature of both icehouse and greenhouse climate states (Boulila et al. 2011).

Here we present a new Late Cretaceous record from the Jordanian Levant Carbonate Platform, comprising a detailed physical-, bio-, chemo- and sequence stratigraphy. Carbonate content of these strata reflects overall sequence stratigraphic development, and demonstrates a dramatic 3<sup>rd</sup>-order-scale oscillation that is also apparent in the  $\delta^{13}\text{C}_{\text{carb}}$  record. An evaluation of the temporal nature of this oscillation is presented, using radioisotopic geochronology from the Geological Timescale 2012 (GTS-2012) (Gradstein et al. 2012), and astrochronologic testing (Meyers et al. 2012a). The results suggest an ~1 Myr long synchronization of sea-level and stratigraphic sequence development, with potential linkages to the global carbon cycle.

The Cenomanian through Turonian period of time provides an exceptional study interval for the evaluation of linkages between sea-level, the carbon cycle, and astronomical forcing/pacing, as it has excellent global coverage of sequence stratigraphic studies (Gale et al. 2002, Schulze et al. 2003, Sharland et al. 2004, Wilmsen 2003) on material that combines hypothesized astronomical cyclicity (Sageman et al. 2006, Voigt et al., 2008, Wendler et al. 2010, Meyers

et al. 2012a) with strong biostratigraphic age control (Gradstein et al. 2012) and a high-resolution  $\delta^{13}\text{C}$  reference curve (Jarvis et al. 2006). Importantly, the studied section represents an intra-shelf depression of the 200 km wide rimmed Levant carbonate shelf (Powell and Mohammed 2011) that yields sufficient accommodation space to preserve a relatively complete and high-resolution chemostratigraphic record and is also shallow enough to provide a conspicuous sequence stratigraphic stacking pattern, making it suitable for our investigation.

## 2. Materials and Methods

### 2.1 Studied section: Setting, biostratigraphy

Section GM3 (Ghawr Al Mazar (Ghor al Mazrar), Jordan: 31° 15' 34" N; 35° 35' 41" E) represents a platform carbonate sequence deposited in an intra-platform basin (the Karak-Silla basin), palaeogeographically, at approximately 100 km distance from the palaeo-coastline of the Arabian Shield. The NW-dipping Levant Carbonate Platform extended over the passive margin of the Arabo-Nubian shield during Cenomanian-Turonian times with the studied section being positioned at about 5 degrees northern latitude. Facies range from open-marine subtidal to supratidal deposits, based on the analysis of a diverse shallow-water benthic association including calcareous algae, rudists, larger benthic foraminifera, oysters, and ostracodes of marine, brackish to hyper saline environments (Powell 1988, 1989, Schulze et al. 2003, 2004, Morsi and Wendler 2010). The intra-platform basin was connected to the open marine environment and only temporarily experienced restricted conditions (algal mudflat deposition, evaporite formation) during regressions. The interbedding of shallow subtidal deposits with short-lived peritidal expressions implies an amplitude of 3<sup>rd</sup>-order sea-level variation consistent with estimates of about 30 m from other regions (Miller et al. 2005, Voigt et al. 2006).

The section starts at the top of the Naur Formation (Figs. 1A, B; 2). The basal part is biostratigraphically constrained to the middle Cenomanian by calcareous nannofossil zone CC10, based on the first occurrence (FO) of *Microrhabdulus decoratus* (Schulze et al. 2004), and ostracod zone I of Morsi and Wendler (2010), which correlates with middle Cenomanian ostracod zone schemes of Israel and North Africa. The

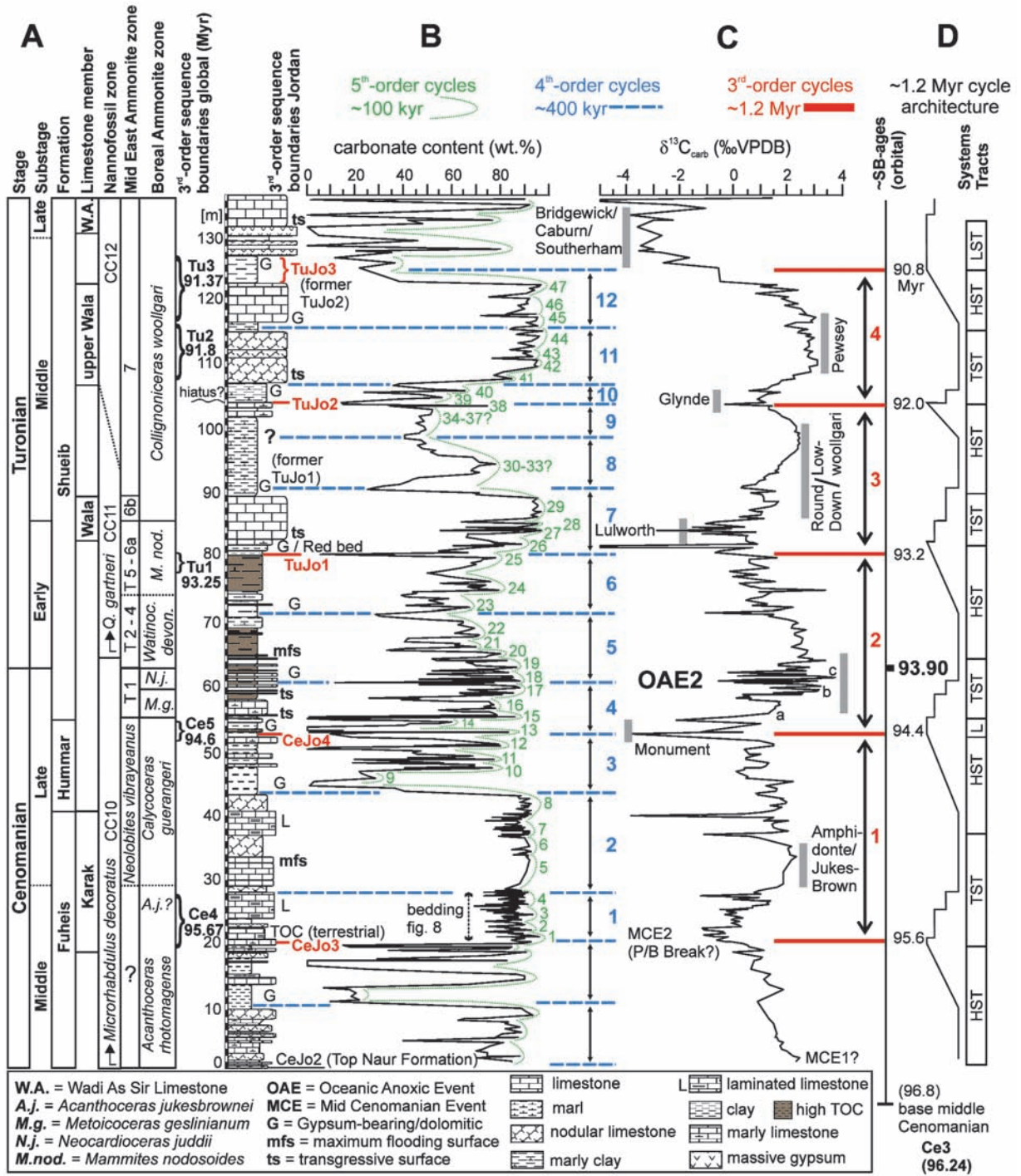
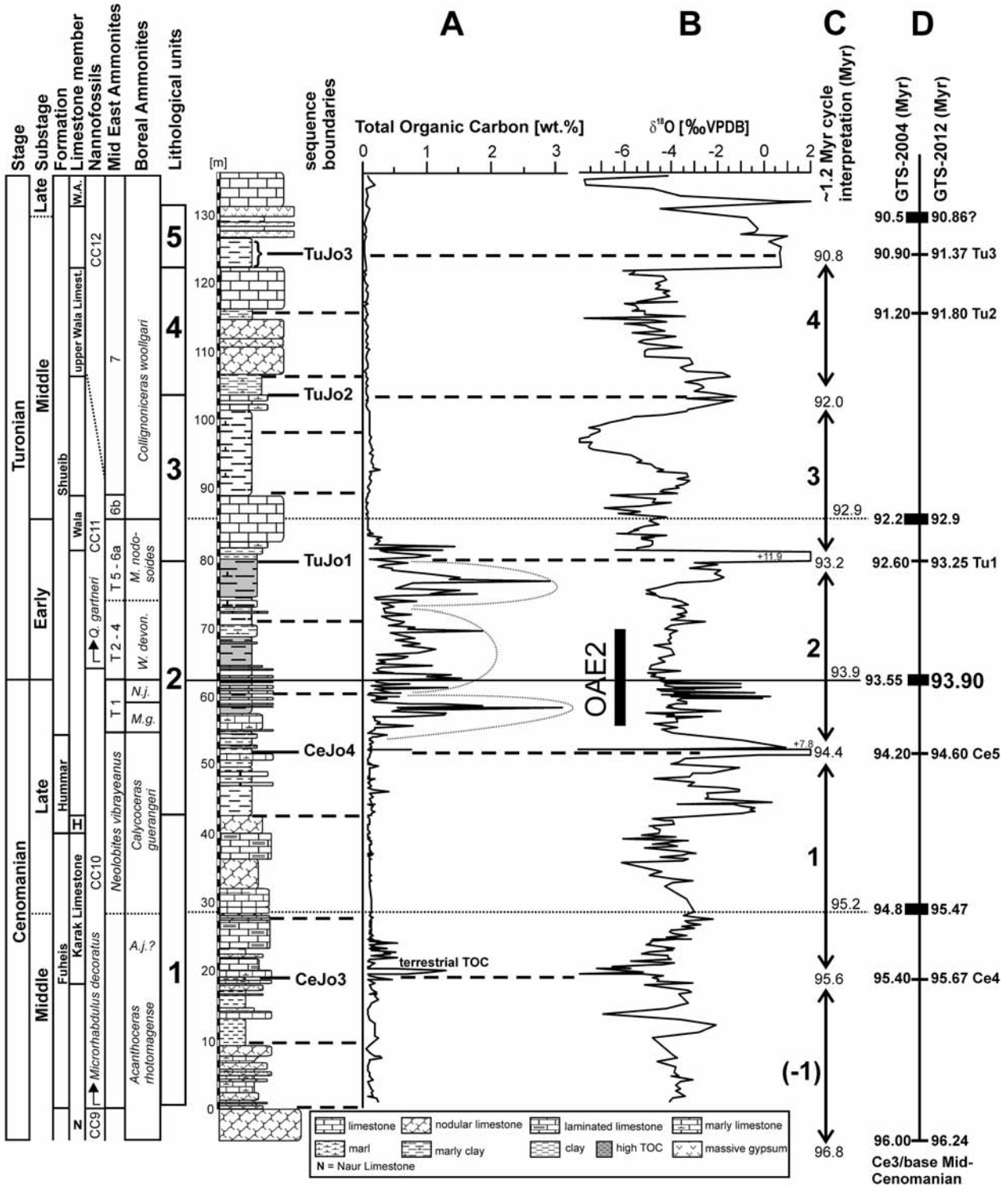


**Fig. 1.** Bio-, litho-, and chemostratigraphy of the studied section along with cyclostratigraphic interpretation. (A) Stratigraphy. Global sequence boundaries (SB) with ages (Gradstein et al., 2012) are shown relative to biostratigraphy and Jordan (Jo) SB, with ranges taking into account differences in the literature and uncertainties in biozone positions in the section (Haq et al. 1987, Hardenbol et al. 1998, Schulze et al. 2003, Wilmsen 2003, Wilmsen et al. 2005, Wendler et al. 2010). (B) wt.%  $\text{CaCO}_3$  and hypothesized 5<sup>th</sup>-order ~100 kyr eccentricity cycles (green, numbered). Hypothesized ~400 kyr eccentricity cycles (blue dashed lines) represent 4<sup>th</sup>-order bundles of 5<sup>th</sup>-order cycles. (C) Bulk carbonate  $\delta^{13}\text{C}$  (events according to Jarvis et al. (2006) are located at turning points in long-term trend and marked with gray bars), long-term  $\delta^{13}\text{C}$  minima mark boundaries of the hypothesized ~1.2 Myr oscillation (red bold lines). Astronomical SB ages are calibrated to the Ar-Ar C/T boundary age of (Meyers et al. 2012b). (D) Sketched cycle architecture of stepwise  $\delta^{13}\text{C}$ -build-ups of the million-year-scale cycle and Systems Tracts (ST): LST-lowstand ST, TST-transgressive ST, HST-highstand ST. See Fig. 7 for detailed section.



location of zone CC10 is also indirectly supported by occurrences of Mid-Cenomanian larger benthic foraminifera in the Naur Formation (Schulze et al. 2003, 2004). The middle/upper Cenomanian boundary is located in the lower part of the Karak Limestone member, based on the FO of *Neolobites vibrayeanus*, which spans the lower upper Cenomanian *Calyco-ceras guerangeri* Zone (Wiese and Schulze 2005). The present cyclostratigraphic analysis begins at the base of the Karak limestone. The Cenomanian-Turonian (C/T) boundary in the middle of the section has strong biostratigraphic control, constrained by the base of nannoplankton zone CC11 (FO of *Quadrum gartneri*), as well as ammonites of the Mid East ammonite biozone T1 and the FO of *Watinoceras* spp. (Wendler et al. 2010). Likewise, the Early/Middle Turonian transition is well constrained by ammonites of the Middle East ammonite biozones T6a/T6b in the Wala Limestone Member (Schulze et al. 2004). Near the section top lies a gypsum marker horizon (Fig. 1) that yields a regional major sequence boundary recognized across the Arabian Plate, and is associated with an uppermost middle Turonian pronounced sea level fall and subsequent onlap (Sharland et al. 2004, Haq and Al-Qahtani 2005), the latter being represented by the onset of the upper Turonian Wadi As Sir Limestone. Above 90 m height within the section, nannofossil zone CC12 is suggested by occurrences of *Eiffellitus eximius* and *Lucianorhabdus maleformis*. Due to substantial differences in the biostratigraphic schemes, owing to both differences in availability of biostratigraphic index fossils, and regionally restricted faunal assemblages, correlation between Jordan, the English Chalk and Pueblo (Colorado, USA) cannot be based on biostratigraphy alone without large uncertainty. Hence,  $\delta^{13}\text{C}$ -isotope stratigraphy is required for chrono-stratigraphic support.

## 2.2 Methods: Geochemistry

The section was sampled at an interval of 10 to 30 cm. A total of 522 samples were measured for carbonate content, total organic carbon (TOC), and bulk carbonate stable carbon and oxygen isotopes. Total organic carbon (wt.% TOC) was measured using a LECO CS-125 Carbon-Sulphur Determinator, and total carbon was determined using a LECO CNS-2000. Carbonate content (wt.%  $\text{CaCO}_3$ ) was calculated using the difference between total carbon and TOC. The analytical precision of reported wt.%  $\text{CaCO}_3$  and wt.% TOC measurements is 1%. Stable carbon and oxygen isotopes were measured on bulk carbonate using a Finnigan MAT 251 mass spectrometer. The results are reported relative to the Vienna Pee Dee belemnite standard (V-PDB) at analytical precision less than  $\pm 0.05\text{‰}$  for  $\delta^{13}\text{C}$  and  $\pm 0.07\text{‰}$  for  $\delta^{18}\text{O}$ . Semi-quantitative cycle analysis is performed using a combined assessment of the carbonate content data and the lithological evidence.

## 2.3 Methods: Time series analysis

A quantitative evaluation of astronomical influence on carbonate platform sedimentation is challenged by the dynamic nature of such environments, including exposure (disconformity) and autocyclic processes (Wilkinson et al. 1996, 1999). To overcome such challenges, and thus provide an objective and exacting test of the astronomical hypothesis that is suitable for the Levant platform data, we implement four specific approaches.

- (1) Available geochronologic constraints from GTS 2012 (Gradstein et al. 2012) are used to assess potential time scales for the oscillations observed in wt.%  $\text{CaCO}_3$  and  $\delta^{13}\text{C}_{\text{carb}}$ .

**Fig. 2.** Stratigraphy, TOC and  $\delta^{18}\text{O}$ . For further stratigraphic information refer to Figure 1. A) Main TOC-rich intervals are at the MCE2 near CeJo3 (terrestrially dominated organic matter) and OAE2 (dominantly marine organic matter (Sepúlveda et al. 2009)). Dotted lines: TOC maxima associated with 4<sup>th</sup>-order (400 kyr eccentricity) cycles. Dashed lines: sequence boundaries. Note strong positive excursions in stable oxygen isotopes (B) at sequence boundaries (CeJo4, TuJo1, TuJo2, TuJo3) suggesting influences of high-salinity brines and meteoric waters (Peryt and Scholle 1996, Wendler, J. E. et al. 2009) that also correspond to the observed evaporites (Gypsum-levels in Fig. 1). C) 3<sup>rd</sup> order cycle boundary ages according to our astronomical interpretation. D) Differences in dating of stage boundary and sequence boundary ages using GTS-2004 (Gradstein et al. 2004) versus GTS-2012 ages (Gradstein et al. 2012) for comparison with ages from the Jordan astronomical interpretation (panel C); the base of the Late Turonian GTS-2012 age – 90.86 Myr is the one associated with the base of the *Subprionocyclus neptuni* Tethyan ammonite zone. It is marked “?” to indicate that an alternative GTS-2012 base Late Turonian age is given in accordance to the U.S. Western Interior Basin ammonite zone *Prionocyclus macombi* at 91.41 Myr. Note that Tu2 and Tu3 previously had GTS-2004 ages which, relative to the new Tu1 age, would correspond well with an interpretation of two ~ 1.2 Myr long sequences (Tu1<sub>GTS-2012</sub>=93.25 Ma to Tu3<sub>GTS-2004</sub>=90.9 Ma ~ 2.35 Myr).

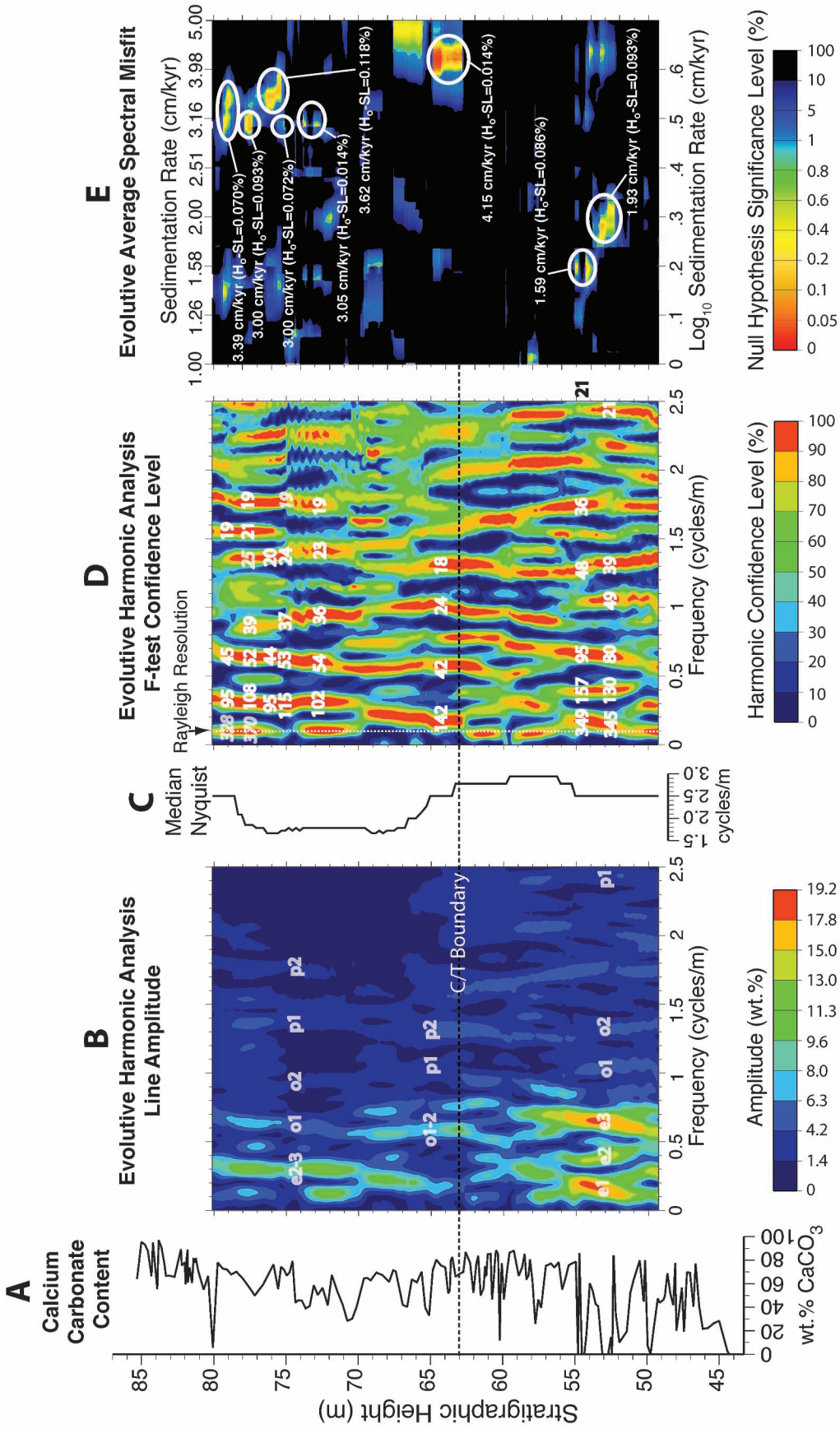


**Fig. 3.** Astrochronologic testing of the interval encompassing OAE2 (44.345–85.305 m) using the astronomical model of Laskar et al. (2011) and Laskar et al. (2004). (A) wt.% CaCO<sub>3</sub>, (B) EHA amplitude results for wt.% CaCO<sub>3</sub>, calculated using 3–2π prolate tapers and a moving window of 10 m (Meyers et al. 2001). The mean value and a linear trend were removed from each 10 m window associated with the EHA. (D) EHA harmonic F-test confidence level results for wt.% CaCO<sub>3</sub>, calculated using 3–2π prolate tapers and a moving window of 10 m. The mean value and a linear trend were removed from each 10 m window. (E) Evolutive-ASM null hypothesis significance levels for the EHA results in panel D. Low values indicate that the null hypothesis of “no astronomical signal” can be rejected with a high degree of confidence. The critical significance level for rejection of the null hypothesis is 0.5% (Meyers and Sageman 2007, Meyers et al. 2012a).

- (2) Evolutive Average Spectral Misfit (E-ASM; Meyers and Sageman 2007, Meyers et al. 2012a) analysis is applied to evaluate wt.% CaCO<sub>3</sub> data from the Cenomanian/Turonian (C/T) boundary interval. The C/T boundary interval is selected because it preserves the deepest marine lithofacies of the studied section, where continuity of sedimentation is most likely to be achieved, and it also constitutes the highest resolution portion of the wt.% CaCO<sub>3</sub> record. Using E-ASM, sedimentologic cycles in the wt.% CaCO<sub>3</sub> data are tested against hypothesized Late-Cretaceous precession (~20 kyr), obliquity (~40 kyr) and eccentricity (~100 kyr, ~400 kyr) variability (Table 1) while considering a range of plausible sedimentation rate models, and the null hypothesis of “no astronomical influence” is quantitatively evaluated using Monte Carlo simulation. The approach permits a null hypothesis test in the absence of rigorous radio isotopic constraints, and is specifically designed for depositional settings characterized by unsteady sedimentation.
- (3) Based on the E-ASM results, a tentative astronomical time scale (ATS) is developed for the C/T boundary interval, spanning 3<sup>rd</sup>-order sequence boundaries CeJo4 and TuJo1 (section 3.2), allowing a quantitative assessment of the duration of this sequence. As a test of the new Jordan C/T ATS, it is compared to the C/T Global Stratotype Section and Point (GSSP) ATS in Colorado (Meyers et al. 2012b), to evaluate the consistency of biostratigraphic and  $\delta^{13}\text{C}$  data between locations (Sageman et al. 2006).
- (4) Lastly, an “ASM minimal tuning” test is conducted, as discussed in section 3.2, to provide a final statistical assessment of the astronomical interpretation provided for the entire ~5 Myr of sedimentation preserved on the Levant platform.

Spectral analyses for the study utilize the multitaper method (MTM; Thomson 1982) with LOWSPEC background estimation (Meyers 2012), and evolutive harmonic analysis (EHA; Meyers et al. 2001); all analyses are conducted with  $3-2\pi$  prolate tapers (Thomson 1982). Prior to spectral analysis, piecewise-linear interpolation is used to place each data series on an even sample grid. To preserve fine-scale structure in the data series, EHA utilizes an interpolation grid that is near the finest observed sample spacing. In contrast, the combined MTM/LOWSPEC approach used in this study can be sensitive to over interpolation, and thus a value near the median sampling interval is used.

EHA and E-ASM for the wt.% CaCO<sub>3</sub> data employ a 10 m window, experimentally determined to provide an optimal assessment of changes in spectral features throughout the stratigraphic record. E-ASM was calculated following equations 1 and 2 of Meyers et al. (2012a). For each 10 m window (Fig. 3D), 200 individual sedimentation rates are evaluated, spanning 1–5 cm/kyr with a logarithmic sedimentation rate scaling. To accommodate the highly variable sample resolution, the median Nyquist frequency for each 10 m analysis window is utilized. Astrochronologic testing evaluates two theoretical astronomical models (Table 1; Berger et al. 1992, Laskar et al. 2004, Laskar et al. 2011).

### 3. Results

#### 3.1 Sequence stratigraphy and carbon isotope results

The section GM3 is part of a sequence stratigraphic framework (Schulze et al. 2004) consisting of thirty four sections covering a 200 km long paleo-bathymetric platform transect. The section is subdivided into five lithologic sequences (Figs. 1, 2). 1) 0–42 m: Alternating oyster-bearing limestone and subtidal clayey marl in the lower part are overlain above CeJo3 by lagoonal algal-laminated limestone followed by open-marine foraminiferal wackestone indicating progressive sea-level transgression. 2) 42–80 m: Highly cyclic deposits of partly restricted environments at the base are followed above CeJo4 by open-marine calcisphere-limestone alternating with organic-rich marls (Fig. 2) including OAE2 (Sepúlveda et al. 2009). The sequence is terminated at TuJo1 by restricted supratidal high-salinity sabkha facies with thin gypsum-rich beds and a shallow-marine red bed (Wendler, J.E. et al. 2009, 2010). 3) 80–103 m: A major flooding is indicated by ammonite- and echinoderm-rich wackestone (Walla Limestone Member) and marl. 4) 103–122 m: Supratidal marl and nodular oyster limestone at the base (TuJo2) are followed by subtidal limestone. 5) 122–131 m: Expanded regression and restricted evaporitic conditions above TuJo3 (corresponding to the Large-Scale Depositional Sequence Boundary SB3 of Powell and Mohammed (2011)) are represented by supratidal clays and massive gypsum beds with chicken-wire textures and tepee-structures. Lithologic indicators of the five 3<sup>rd</sup>-order sequence boundaries (Fig. 1) are signs of shallowing represented by the sabkha deposits (CeJo4, TuJo1, TuJo2, TuJo3) and a

laminated limestone-marl-succession that yields terrestrial organic carbon (Fig. 2A, CeJo3) including coal-debris. Global sequence boundaries (Fig. 1A) with GTS-2012 ages (Gradstein et al. 2012) have been correlated to the present section relative to biostratigraphy, and correspond to the Jordan sequence boundaries, with ranges taking into account differences in the literature and uncertainties in biozone positions in the section (Haq et al. 1987, Hardenbol et al. 1998, Schulze et al. 2003, Wilmsen 2003, Wilmsen et al. 2005, Wendler et al. 2010).

Five major  $\delta^{13}\text{C}$  minima (Fig. 1C) occur synchronously with the identified sequence boundaries (Fig. 1B) partitioning the  $\delta^{13}\text{C}$  record into four large-scale oscillations. Each of these cycles has a steep, two or three phase  $\delta^{13}\text{C}$  build-up associated with a transgressive surface followed by a plateau and a slow decrease (Fig. 1D). Stratigraphic horizons associated with higher-order shallowing events (bold dashed lines in Fig. 1) show small enrichments of gypsum, algal mudflat deposits (laminated limestone), or are omission surfaces at limestone tops, and are frequently related to minor  $\delta^{13}\text{C}$  minima.

The Jordan  $\delta^{13}\text{C}$  record provides an important correlation tool that, in its large-scale oscillation, preserves all of the major features observed in the Late Cretaceous reference curve (named events in Fig. 1C; Jarvis et al. 2006). The base of the section captures the upper part of the MCE1, followed by a marked negative  $\delta^{13}\text{C}$  spike (MCE2 or P/B Break). The  $\delta^{13}\text{C}$  data also reflect the Jukes-Brown, Monument, OAE2, Lulworth, Round Down/Low woollgari, Glynde and Pewsey  $\delta^{13}\text{C}$  events of Jarvis et al. (2006). The section top comprises a broad trough in carbon isotopic values, which we correlate to the broad  $\delta^{13}\text{C}$  trough associated with the English Chalk Southerham, Caburn and Bridgewick-Events (Jarvis et al. 2006). It is important to consider that, while the mentioned  $\delta^{13}\text{C}$ -events named in the English Chalk reference curve (Jarvis et al. 2006) are based on specific local event beds, they are positioned at major long-term minima or maxima that are clearly documented in the Jordan record. These features in long-term trend within both the English Chalk and the Jordan record are consistent, while obviously differing in detailed shape.

Recent global comparison of  $\delta^{13}\text{C}$  data including the Turonian time interval (Wendler 2013) corroborates that records of very different shapes can share the same long-term features, supporting use of these features as correlation tools. It must also be noted that the large magnitude of the  $\delta^{13}\text{C}$  events in the Jordan record ne-

cessitates local depositional/diagenetic influences. For example, pronounced  $\delta^{13}\text{C}$  minima can be interpreted as due to the influence of soil-derived  $\text{CO}_2$  (Elrick et al. 2009, Immenhauser et al. 2008), consistent with depleted  $\delta^{18}\text{O}$  values (Fig. 2B) from enhanced meteoric water contribution (e.g., MCE2 in Figs. 1 and 2, Knauth and Kennedy 2009). Interestingly, carbonate platform  $\delta^{13}\text{C}$  records of the OAE2 from Mexico (Elrick et al. 2009) show an almost identical double-peaked, high magnitude negative excursion preceding OAE2. Such  $\delta^{13}\text{C}$  values have alternatively been shown to represent stable isotope signatures from high-salinity brine – meteoric mixing environments (Allen and Matthews 1982, Peryt and Scholle 1996, Wendler, J.E. et al. 2009), also associated with strong positive excursions in stable oxygen isotopes, as observed in the Jordan data from CeJo4, TuJo1 and TuJo3 (Fig. 2B). This is in agreement with inferred sea-level regression but, due to probable omission-caused hiatuses at the sequence boundaries, it imparts some ambiguity upon the temporal relationship between the Jordan and global  $\delta^{13}\text{C}$  signal on time scales in the 10–100 kyr range. Additionally, late diagenetic overprint of the SB-levels must be considered, especially at the major lithological changes at the bases of the limestone members.

### 3.2 Cyclostratigraphic evaluation

Geochronologic constraints provided by the GTS-2004 and GTS-2012 (Gradstein et al. 2004, Gradstein et al. 2012) reveal that the observed large scale oscillation in  $\delta^{13}\text{C}$  data, wt.%  $\text{CaCO}_3$ , and stratigraphic architecture is on the order of  $\sim 1$  Myr (Figs. 1C, 2C). To further constrain the chronology and provide a quantitative evaluation of the observed oscillatory variability, we perform astrochronologic testing on the Levant Platform wt.%  $\text{CaCO}_3$  record using the recently developed inverse method of Evolutive Average Spectral Misfit (E-ASM) (Meyers and Sageman 2007, Meyers et al. 2012a). We apply the technique to the highest resolution portion of the wt.%  $\text{CaCO}_3$  record (section meter 45–85), which is most likely to accurately record the high-frequency astronomical (precession and obliquity) terms if present. The objective of the first phase of this analysis is to determine if it is possible to develop a high-resolution astronomical timescale (Figs. 3, 4, 5, 6) to evaluate the amount of time elapsed between 3<sup>rd</sup>-order sequence boundaries CeJo4 and TuJo1, which bracket OAE2 (Fig. 1).

The analyses identify a significant astronomical signal within the OAE2 interval (Fig. 3; results from



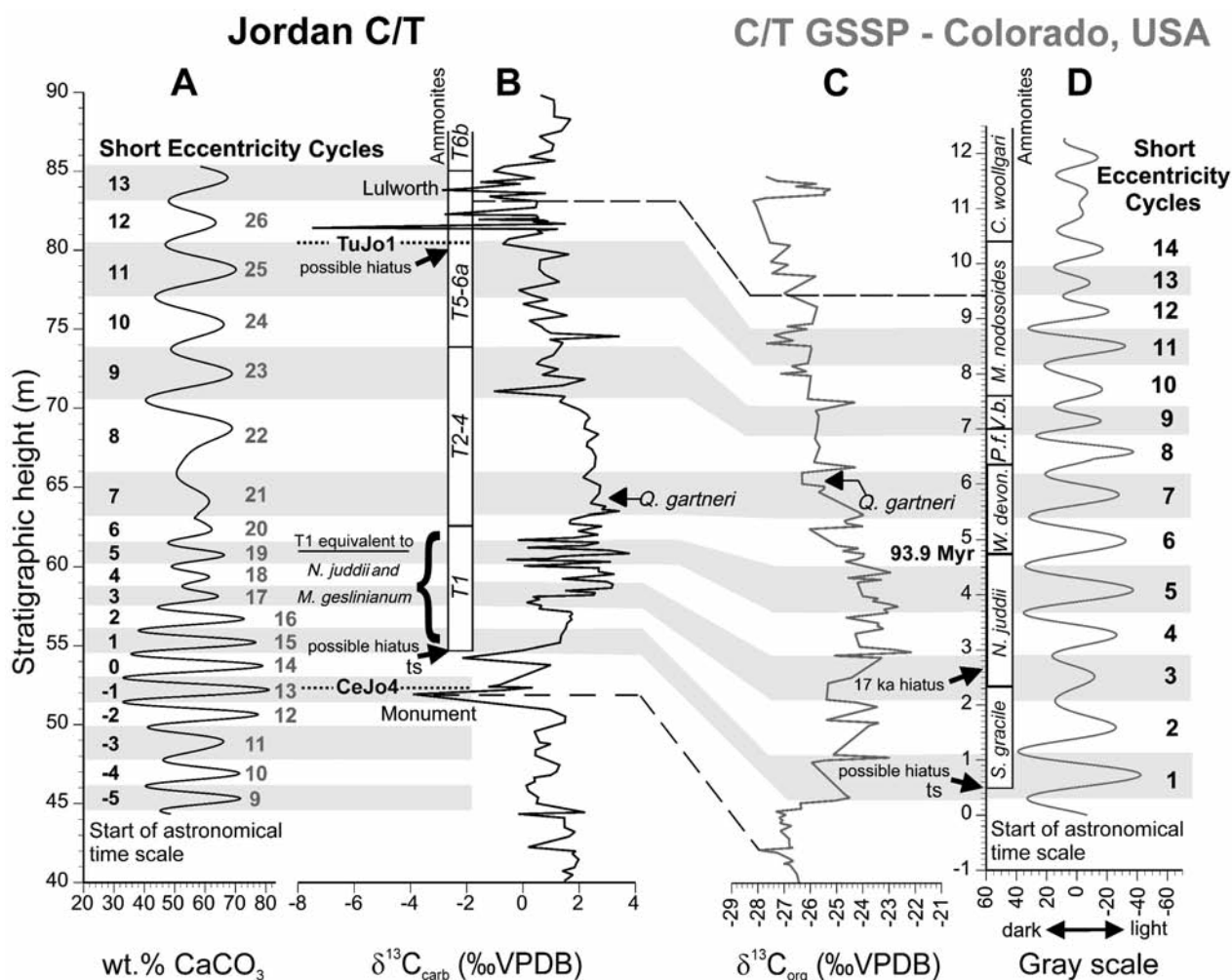


**Fig. 4.** Correlation of astronomical time scales between Jordan and the Cenomanian-Turonian Global Stratotype Section and Point (C/T GSSP, Pueblo, Colorado, USA). (A) Short eccentricity cycle extracted via bandpass filtering of the Jordan wt.% CaCO<sub>3</sub> data (filtering utilizes a 10% cosine window with a frequency range of 0.5–0.8 cycles/m below ~63 m, and 0.15–0.4 cycles/m above ~63 m); gray numbers correspond to the numbering of 5<sup>th</sup>-order cycles in figs. 1B and 7. (B) δ<sup>13</sup>C<sub>carb</sub> record from Jordan, and ammonite biozones T1, T2–4, T5–6a, 6b. (C) δ<sup>13</sup>C<sub>org</sub> record from the U.S.G.S. #1 Portland core near the GSSP, after Sageman et al. (2006). (D) Short eccentricity cycle extracted via bandpass filtering of gray scale record from the U.S.G.S. #1 Portland core, along with ammonite biozones, (after Meyers et al. 2012b). The Jordan record and the GSSP are initially correlated on the basis of a one-to-one match of short eccentricity cycles starting at the beginning of the positive δ<sup>13</sup>C isotope excursion, which results in good agreement with the broad scale pattern of the δ<sup>13</sup>C data and biozone correlation. No high-resolution correlation of the δ<sup>13</sup>C data is implied. ts = transgressive surface.

the Laskar model are presented, but the Berger model yields similar results). A doubling in sedimentation rate above the C/T boundary (Fig. 3) is observed using E-ASM, consistent with drowning of the Tethyan carbonate platforms due to sea-level rise, which resulted in increased accommodation space. Similar increases in sedimentation rate across the C/T boundary have been observed at Tarfaya (Morocco) and Demerara Rise using E-ASM (Meyers et al. 2012a), indicating a wider regional significance of this phenomenon. Inter-

estingly, the change in sedimentation near the C/T boundary in section GM3 is sufficient to result in a near alignment of different astronomical components above and below the boundary, resulting in a “cryptic” sedimentation rate change that would have likely been overlooked without the application of E-ASM.

As a further test of the new Jordan astronomical time scale (ATS), we compare it to the C/T GSSP ATS (Colorado, USA) using biostratigraphy and the δ<sup>13</sup>C data (Fig. 4). Here, the cyclostratigraphic records from

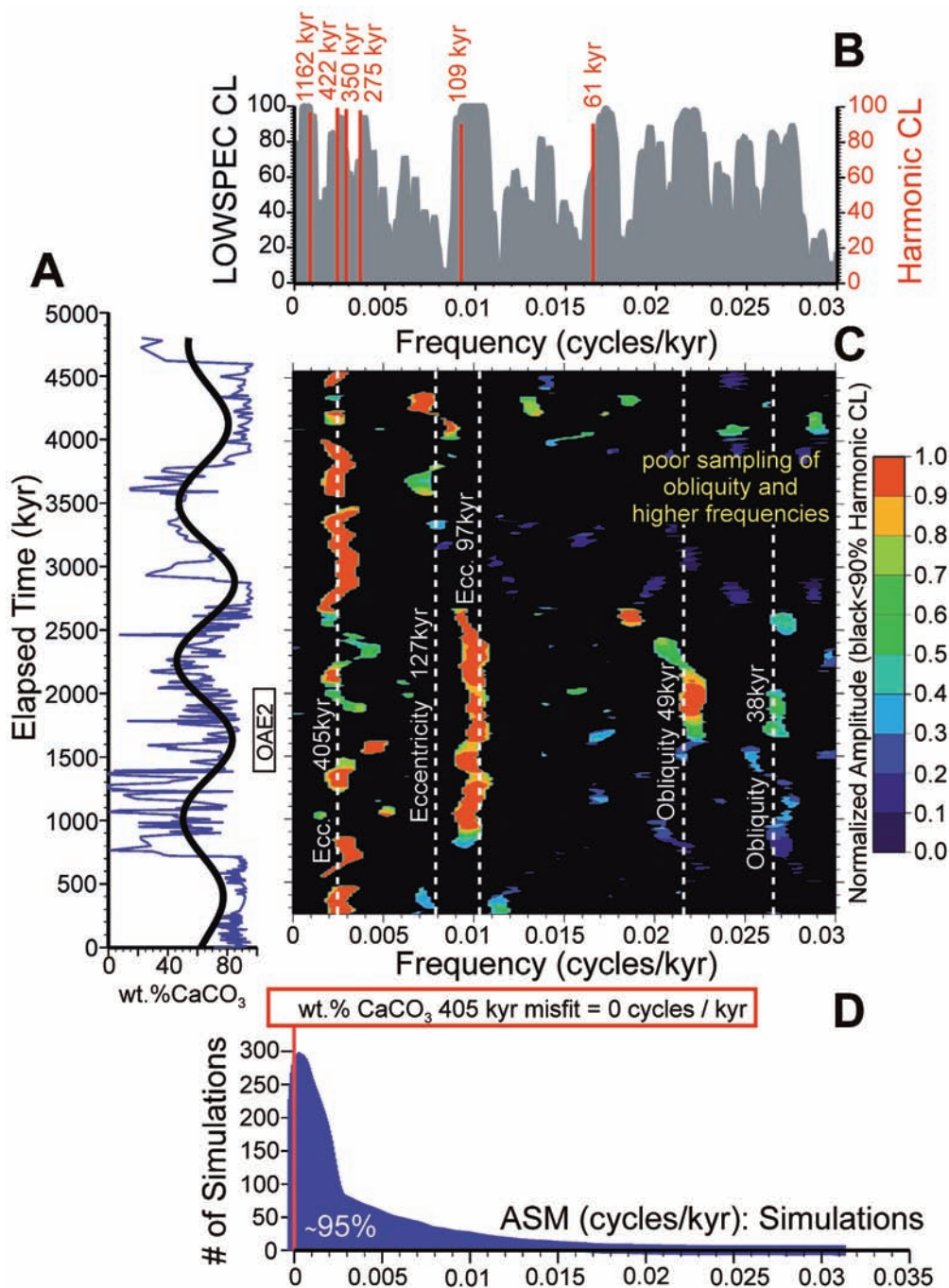


**Fig. 5.** Astrochronologic testing of the minimally-tuned wt.% CaCO<sub>3</sub> data. (A) Minimally tuned wt.% CaCO<sub>3</sub> data with the bandpass filter output for the ~1.2 Myr cycle. (B) LOWSPEC (Meyers 2012) background noise confidence levels and MTM harmonic F-Test (Thomson 1982) results determined using 3–2 $\pi$  prolate tapers. As a component of the LOWSPEC analysis, the data series was prewhitened using an AR(2) filter, objectively determined as outlined in Thomson et al. (2001). The harmonic F-Test peaks identified in panel B pass the criteria outlined in Meyers (2012), specifically designed to decrease false positive rate (one of the significant frequencies occurs at 0.0335 cycles/kyr, and thus is not displayed; the Nyquist frequency is ~0.042 cycles/kyr). (C) Evolutive Harmonic Analysis (EHA) of the minimally-tuned wt.% CaCO<sub>3</sub> data using 3–2 $\pi$  prolate tapers, and a moving window of 500 kyr. The mean value and a linear trend have been removed from each 500 kyr window. As in Meyers and Hinnov (2010), amplitude results have been normalized such that the maximum amplitude in each 500 kyr window is unity, and have been filtered at the 90% harmonic F-test confidence level (areas in black are not significant). (D) Monte Carlo simulation results for the ASM minimal-tuning test, indicating that ~95% of simulations exceed the observed misfit of 0 cycles/kyr associated with the hypothesized 405 kyr long eccentricity cycle.

each site are anchored at the initiation of the positive carbon isotope excursion, and the short eccentricity cycles are then matched to provide a hypothesis for correlation, which can subsequently be evaluated with the biostratigraphy and  $\delta^{13}\text{C}$  chemostratigraphy. Overall, this indicates excellent agreement within available constraints: (1) Middle East ammonite biozone T1 occurs contemporaneously with *S. gracile* and *N. juddi* in Colorado, (2) the first occurrence of *Q. gartneri* occurs in the same eccentricity cycle at both sites, and (3) the “Lulworth” negative  $\delta^{13}\text{C}$  excursion at Jordan maps into the upper *M. nodosoides* ammonite biozone in Colorado, as is the case at Dover and Culver Cliff in England (Jenkyns et al. 1994, Jarvis et al. 2006; note that the negative  $\delta^{13}\text{C}$  excursion is not obvious in Colorado, but data resolution is low). While these results do provide support for the Jordan ATS, it should be noted that variable  $\delta^{13}\text{C}$  resolution and uncertainties in the relationship between ammonite zonations on the two continents provide ambiguities in portions of the records (Fig. 4).

Using the new ATS from Jordan (based on the short-eccentricity cycle) we observe that the established 3<sup>rd</sup>-order sequence boundaries (CeJo4 and TuJo1) are separated by  $\sim 1.2$  million years (Figs. 1, 4, 5, 6), suggesting a possible link between eustatic sea-level, a cyclic driver that potentially is the Earth’s long-term obliquity modulation, and the global carbon cycle. Based on this result and supporting radio-isotopic data (Gradstein et al. 2012), we hypothesize that the other observed 3<sup>rd</sup>-order sequence boundaries are paced in a similar manner. However, the highly variable lithology (e.g., wt.%  $\text{CaCO}_3$ ) and data resolution above and below OAE2 make evaluation of the high-frequency precession and obliquity cycles challenging to impossible, hindering the use of E-ASM through these intervals. Thus, we employ an alternative approach and develop a tentative time scale that extends above and below the OAE2 short eccentricity ATS using the 3<sup>rd</sup>-order sequence boundaries as markers of the proposed  $\sim 1.2$  Myr cycle (Figs. 5A, 6), then we quantitatively evaluate if this “minimal tuning” brings into focus the expected higher-resolution astronomical terms associated with eccentricity (and obliquity where resolution permits). The tuning utilizes only three additional tie points, thus it is highly conservative.

Time-frequency analysis of the resultant tuned wt.%  $\text{CaCO}_3$  data identifies relatively persistent cycles that are consistent with long eccentricity (405 kyr; Fig. 5B, C; 6), exceeding the 90% confidence level of both the MTM harmonic F-test (Thomson 1982) and

LOWSPEC noise background (Meyers 2012) for the entire minimally tuned record (Figs. 5B, 6). Not surprisingly, short eccentricity, which was utilized as a tuning frequency for a portion of the wt.%  $\text{CaCO}_3$  record (770 kyr–2570 kyr), also exceeds the 90% confidence level (Fig. 5B, C). Importantly, the short-eccentricity tuning also independently brings into focus the obliquity terms (38, 49 kyr) through the OAE2 interval (Fig. 5C). Time-frequency analysis (Fig. 5C) indicates the presence of short-eccentricity scale variability above the OAE2 interval, where it drifts to periods more consistent with an expected 127 kyr cycle (Laskar et al. 2011). Further evidence in support of the minimal tuning comes from the observation that short eccentricity variability is strong in the OAE2 interval when long eccentricity variability is weak (Fig. 5C), and vice versa, a feature that is pervasive in the theoretical astronomical models (Laskar et al. 2004, Laskar et al. 2011).

As a final step in our quantitative evaluation, a new adaptation of the ASM technique is used to explicitly evaluate the probability that the observed long-eccentricity signal misfit (0 cycles/kyr given the spectral resolution) would arise by chance alignment of a ‘false positive’ in the minimally tuned record (Vaughan et al. 2011, Meyers 2012). The “ASM minimal-tuning test” is only valid for astronomical periods that have been excluded from the tuning exercise, and is also limited by variable sampling resolution. Specifically, based on E-ASM results a short eccentricity tuning has been imposed between sequence boundaries CeJo4–TuJo1, and the other 3<sup>rd</sup>-order sequence boundaries have been assigned a 1.2 million year recurrence interval. Furthermore, sampling resolution prohibits continuous assessment of precession and obliquity scale variability throughout the stratigraphy. Given these constraints, the long-eccentricity cycle (405 kyr) is the only term available for the minimal-tuning test. Since long-eccentricity is considered the most stable period of the Phanerozoic (Laskar et al. 2004, Laskar et al. 2011), it provides an ideal astronomical term for our evaluation.

Significant wt.%  $\text{CaCO}_3$  temporal periods for the ASM minimal-tuning test are identified using a robust locally weighted regression estimate of the spectral background (LOWSPEC; (Meyers 2012) and the MTM harmonic F-test, as discussed in (Meyers 2012) (Fig. 5B). Specifically, significant F-test peaks must simultaneously achieve the 90% harmonic F-test confidence level, and also the 90% LOWSPEC confidence level within  $\pm$  half of the power spectrum bandwidth resolution ( $\pm 1/2382 \text{ kyr}^{-1}$ ), while also

Table 1 Theoretical target periods used in the ASM analyses, based on the time domain astronomical model of Laskar et al. (2004, 2011) and the frequency domain astronomical model of Berger et al. (1992). Please see Meyers et al. (2012a) for details regarding estimation of mean values and uncertainties.

Term	Mean LA04/LA11 frequency (cycles/kyr)	$N\delta$	Corresponding Laskar04/Laskar11 period (kyr)	$2\sigma$ uncertainty (cycles/kyr)	% Uncertainty in frequency	Berger et al. (1992) period (kyr)
E1	$2.466250 \times 10^{-3}$	4	405.47	$5.737305 \times 10^{-5}$	2.3%	*
E2	$7.875000 \times 10^{-3}$	8	126.98	$3.585686 \times 10^{-4}$	4.6%	*
E3	$1.031875 \times 10^{-2}$	8	96.91	$4.307386 \times 10^{-4}$	4.2%	*
O1	$2.060000 \times 10^{-2}$	4	48.54	$3.265986 \times 10^{-4}$	1.6%	50.43
O2	$2.655000 \times 10^{-2}$	4	37.66	$2.000000 \times 10^{-4}$	0.8%	38.93
P1	$4.460000 \times 10^{-2}$	4	22.42	$1.566312 \times 10^{-3}$	3.5%	22.34
P2	$5.455000 \times 10^{-2}$	4	18.33	$2.000000 \times 10^{-4}$	0.4%	18.54

$\delta$  = number of estimates used for determination of mean frequency and standard deviation.

\* = Berger et al. (1992) do not provide Cretaceous eccentricity period estimates. The eccentricity periods of Laskar et al. (2011) are used.

occurring on a local power spectrum high. These criteria are implemented to reduce the false positive rate, while also being sensitive to the limitations of cyclostratigraphic data (Meyers 2012).

Seven frequencies in the minimally tuned wt.%  $\text{CaCO}_3$  spectrum satisfy the criteria outlined above (Fig. 5B; one of the significant frequencies occurs at 0.0335 cycles/kyr, and thus is not displayed in the figure). Given the resolution of the wt.%  $\text{CaCO}_3$  spectral estimate, and the uncertainties in the theoretical long-eccentricity period (Table 1), the spectral misfit between the predicted 405 kyr (396–415 kyr) and observed 422 kyr (404–441 kyr) cycle is 0 cycles/kyr. To determine the probability that this misfit would arise by chance alignment of a ‘false positive’ spectral peak, 100,000 Monte Carlo spectra were generated using 7 frequencies distributed at random frequencies, each with identical spectral resolution as the measured wt.%  $\text{CaCO}_3$  spectrum. In total, only 5.335% of the simulations achieve a spectral misfit of 0 cycles/kyr (p-value = 0.05335), indicating that we can reject the null hypothesis of chance alignment at the ~95% confidence level (Fig. 5D). It should be noted that this confidence level is not subject to a ‘multiple-test’ correction, and thus reflects the true probability of rejecting the null hypothesis in error (see discussion in Meyers 2012).

To complement the spectral results presented above, a semi-quantitative assessment of bedding rhythms based on the lithological evidence and carbonate content is conducted (Fig. 1A, B; Fig. 7 for detailed chemostratigraphic log) and calibrated to time according to GTS-2012 age estimates. Relevant for our as-

essment is the timespan between global sequence boundaries Ce4 and Tu3 as it comprises the four full oscillations defined by major 3<sup>rd</sup>-order sequence boundaries and corresponding  $\delta^{13}\text{C}$  minima (Fig. 1C). This interval is ~4.3 Myr long (GTS-2012) (Figs. 1, 2D), and thus each of the four oscillations spans ~1.1 Myr, if they are of equal duration. In addition to the main sequence boundaries, a higher-frequency repetition of gypsum-bearing, dolomitic marly limestone and clay beds or algal laminated limestone tops related to sea-level lowstands is present (Fig. 1B – 4<sup>th</sup>-order cycles) and is frequently associated with minor  $\delta^{13}\text{C}$  minima. These bed stacks partition each ~1.1 Myr cycle into three sub-cycles (marked with dashed lines in Fig. 1B). Notably, in 3<sup>rd</sup>-order sequence 2, containing the OAE2 and related enhanced TOC values (Fig. 2A), the three 4<sup>th</sup>-order cycles are also reflected in the TOC record. These cycles in TOC are suggestive of productivity maxima associated with the 4<sup>th</sup>-order transgressions. Within the analyzed section-interval of ~4.3 Myr, twelve such bed stacks are distinguishable. This implies a duration of ~358 kyr for one such potential cycle, if they are of equal duration.

Based on E-ASM results the short eccentricity cycle (~100 kyr) is preserved with spatial periods of 1.59–4.15 m (Figs. 3, 4) through the OAE2 interval and corresponds to couplets of limestone beds alternating with marly limestone, marl or clay layers, also apparent in the carbonate content record in figures 1B and 7 (couplets 13–25). Within the ~4.3 Myr interval from CeJo3 to TuJo3 we observed 47 such couplets (Figs. 1, 7), i.e. ~91 kyr per couplet, with uncertainties due to poor bedding in the marl interval between section

meters 90–130. This sedimentological assessment of the higher order cyclicity (the proposed  $\sim 400$  kyr and  $\sim 100$  kyr cycles) throughout the section incorporates a degree of subjectivity in lithologic cycle identification (Figs. 7, 8), and it reveals a noisy record, not unexpected given the dynamic nature of carbonate platform environments, but the quantitative time-series analyses support the inference of a robust astronomical signal nonetheless (Figs. 3–6).

## 4. Discussion

### 4.1 Implications for stratigraphy

Our analysis refines the sequence stratigraphic framework of the Levant Platform in that some of the previously proposed 3<sup>rd</sup>-order sequence boundaries (Schul-

ze et al. 2003) that were inferred based primarily on pronounced sedimentary surfaces (CeJo2, TuJo1) appear to actually be higher-order cycle boundaries that are probably enhanced due to local effects (Fig. 1). Likewise, the cycle bounded by global sequence boundaries Tu2 and Tu3 (GTS-2012 duration 430 kyr) potentially represents a 400 kyr cycle of our astronomical interpretation (4<sup>th</sup>-order cycle 12, Fig. 1), while the global sequences Ce4–Ce5 (1.07 Myr) and Ce5–Tu1 (1.35 Myr) do have, within error, GTS-2012 duration estimates in line with a hypothesized  $\sim 1.2$  Myr cycle (Figs. 1, 2D). These observations indicate that the sharpness of sedimentary surfaces used for sea-level reconstruction is not necessarily linked to the hierarchy of the cycles they represent, which can explain discrepancies between sequence stratigraphic schemes in distant locations. Such ambiguities are to be expected

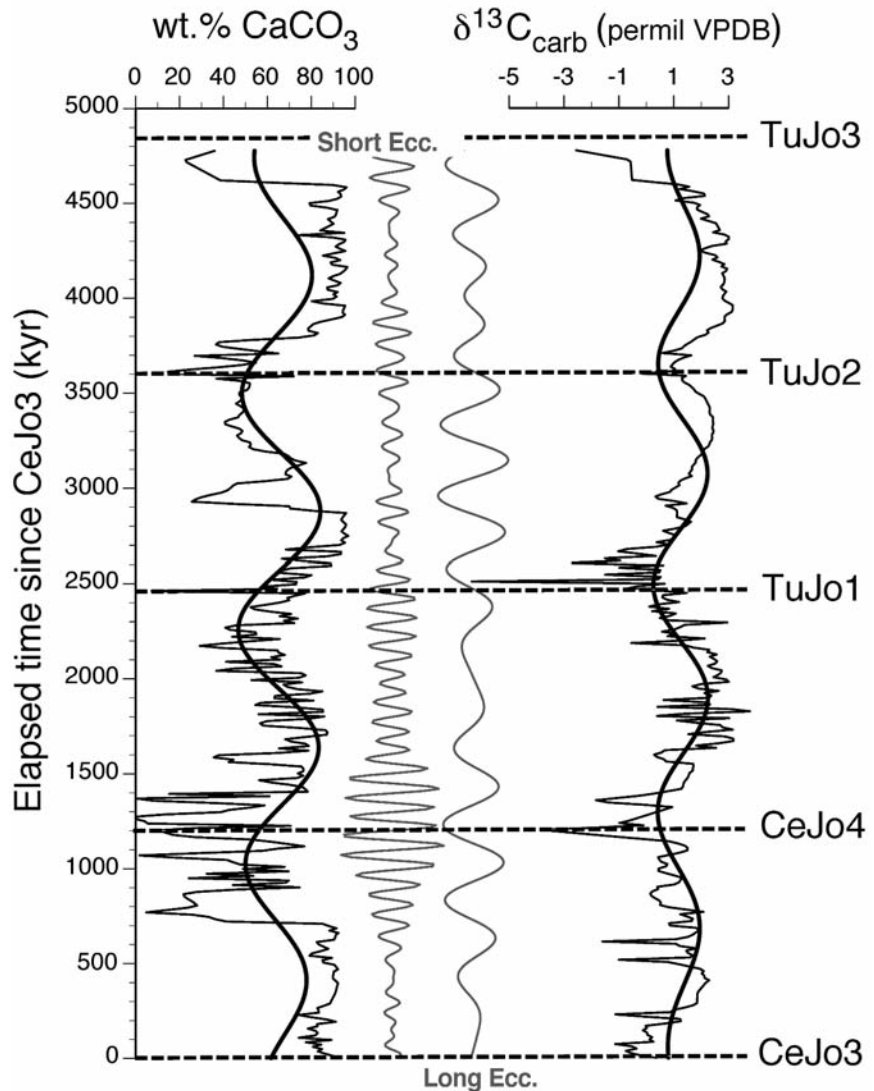


**Fig. 6.** Bandpass filtered minimally-tuned records for wt.% CaCO<sub>3</sub> and δ<sup>13</sup>C, with sequence boundaries identified. Bandpass analysis utilizes a 30% cosine window, with the following bandpass frequency ranges: 0.002–0.0032 cycles/kyr (long eccentricity), 0.065–0.12 cycles/kyr (short eccentricity), 0.00064–0.00105 cycles/kyr ( $\sim 1.2$  Myr oscillation). Short and long eccentricity bandpass results are only displayed for the minimally-tuned wt.% CaCO<sub>3</sub> record.

■ bed boundaries confirmed by field observation and %carbonate lows

▨ beds of increased carbonate content

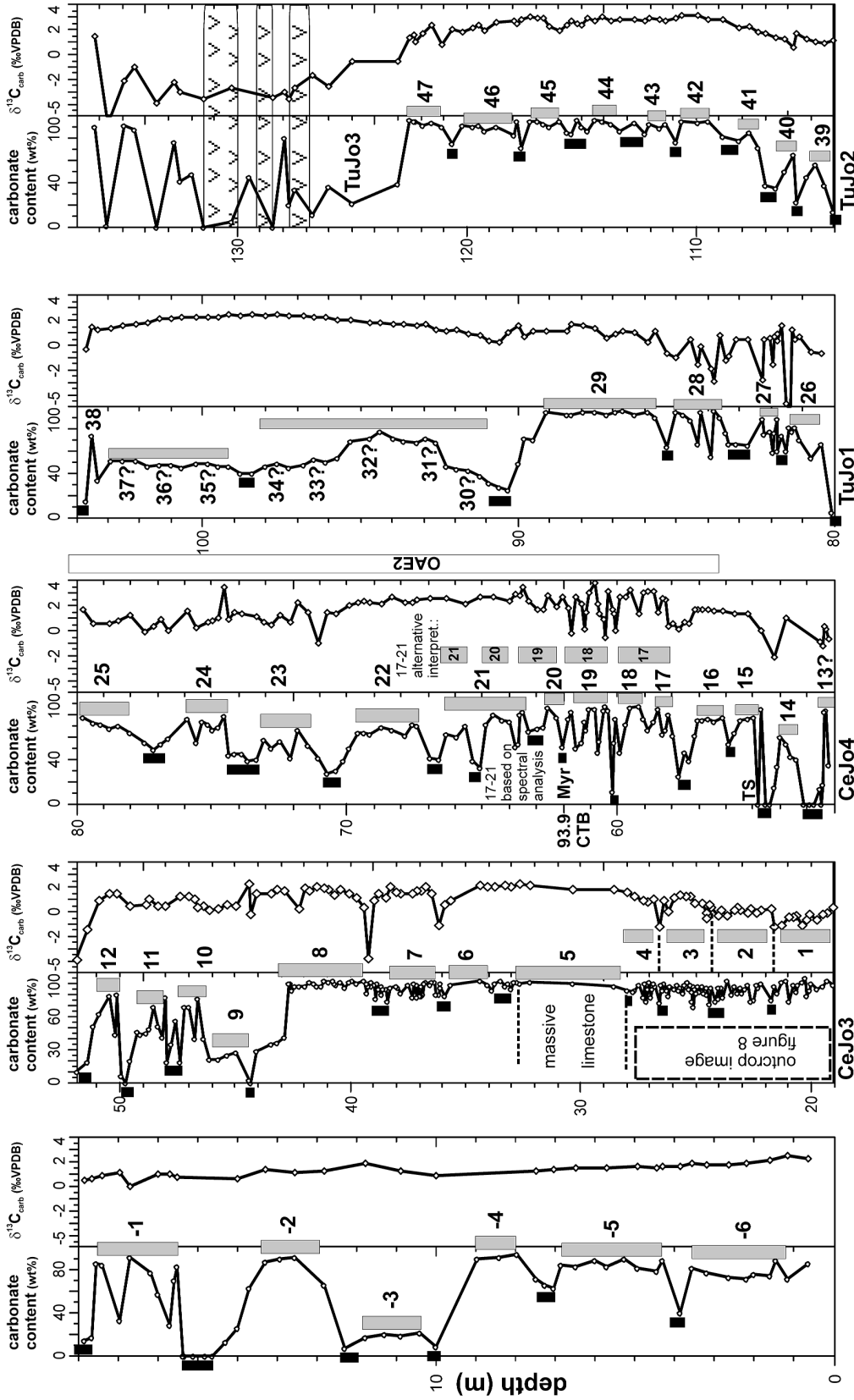


**Fig. 7.** High-resolution illustration of the chemostratigraphic log; the section is divided into parts using the positions of the 3<sup>rd</sup>-order sequence boundaries. Beds (and bundles) are distinguished based on field observation and wt. % CaCO<sub>3</sub>. Note that in the wt. % CaCO<sub>3</sub> record, higher-order carbonate fluctuation may obscure bundles and lead to ambiguities, e.g. bundles 1–4 which are visually obvious (Fig. 8). Also note alternative options for interpretation in the platy limestone bundles 17–21 (OAE2). Above TuJo3 note massive gypsum beds marking the pronounced latest mid-Turonian lowstand interval.

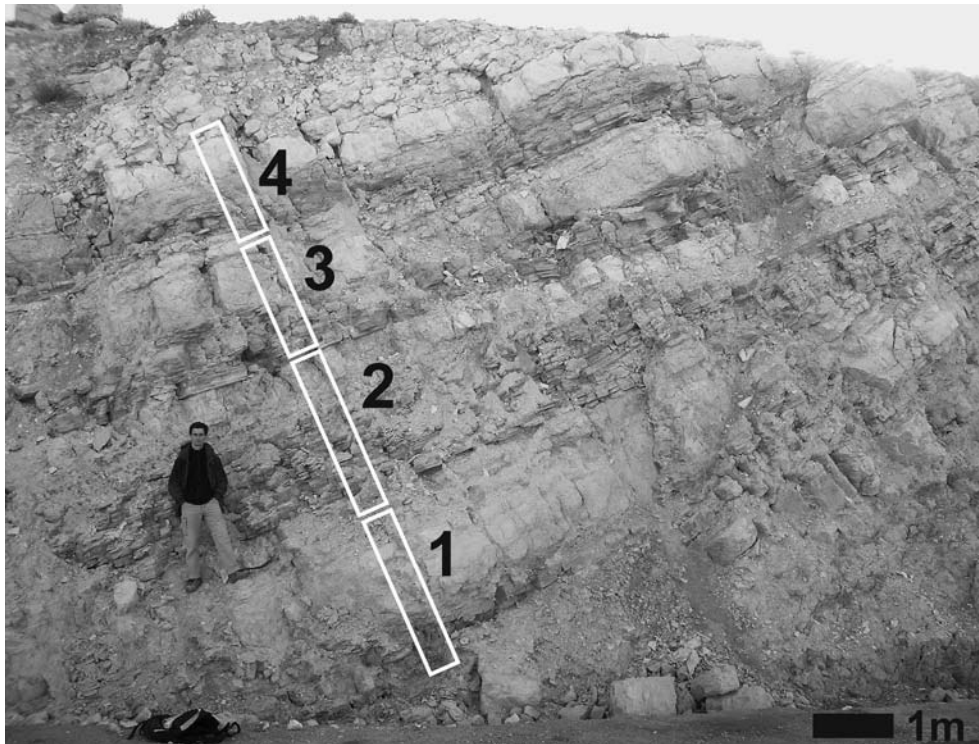


**Fig. 8.** Outcrop image of the lower Karak Limestone showing bundles 1–4 (numbers correspond to Fig. 1) which are located above CeJo3, and are not obvious in the wt.% CaCO<sub>3</sub> record alone (compare to Figs. 1 and 7, which also indicate the stratigraphic position of the imaged portion of the section).

when one considers that any stratigraphic succession represents global eustatic forcing, local accommodation space changes due to subsidence, tectonic uplift, and changes in sediment supply.

Furthermore, our new findings from the Levant Platform have implications for revision of the geological time scale. In particular, according to the astronomical interpretation of section GM3 the approximate age of the Early/Mid Turonian boundary (Fig. 2D) differs by ~700 kyr from the GTS-2004 (Gradstein et al. 2004) stage boundary age. Interestingly, similar age discrepancies for the Lower/Mid Turonian transition of the same magnitude (~600 kyr) are consistently revealed by other astronomical model approaches based on precessional-, short- and long-eccentricity cycle analyses of the OAE2 interval (Sageman et al. 2006, Voigt et al. 2008, Wendler et al. 2010). The new early/mid Turonian boundary age (Gradstein et al. 2012) is now in line with these and the present astronomical interpretations (Fig. 2D).

Another age difference relative to both GTS-2004 and GTS-2012 is suggested by our interpretation at the MCE1, although we cannot provide a specific estimate

due to the partial representation of MCE1 at the section base. The Levant Platform astronomical interpretation suggests the amount of time from the base of the section through the CTB is ~2.5 Myr, and it predicts a third 400 kyr cycle to complete the lowermost sequence towards sequence boundary Ce3, which is associated with the base of the Middle Cenomanian. The resulting duration of ~2.90 Myr for the duration of the Mid- and Late Cenomanian contrasts with the GTS-2012 estimate (2.34 Myr) but is in line with the astronomical approach of Gale et al. (1999), which is based on long eccentricity and precession-forced sedimentation of chalk-marl couplets. Their model assigns a 200 kyr higher age to the first occurrence of *Acanthoceras rhotomagense* (see also figure 8 in Voigt et al. 2008), and estimates the duration of the entire Mid- and Late Cenomanian to be ~3.0 Myr.

In summary, resolving the discussed sequence stratigraphic and age discrepancies using quantitatively constrained astronomical interpretations has a profound impact on the global correlation of sequence boundaries, and it facilitates refinements necessary to eliminate ambiguities in geological dating.

## 4.2 Potential coupling of sea-level, the carbon cycle and astronomical influence

Previous work has noted a strong correspondence between eustatic sea-level and  $\delta^{13}\text{C}$  in the Cretaceous, utilizing a composite record from the English Chalk and published sea-level curves from Russia, India and NW Europe (Jarvis et al. 2006). This coupling has been interpreted to reflect transfer of organic matter into the geosphere in the area of shallow shelf during sea-level rise. The new data set from Jordan also suggests that 3<sup>rd</sup>-order relative sea-level changes of the late Cretaceous Levant Platform and the carbon cycle oscillate synchronously at an approximate million-year time scale, potentially linked to obliquity modulation. However, an analysis of the detailed linkage between eustasy and the global carbon cycle requires de-convolution of local sea-level related influence on the  $\delta^{13}\text{C}$  record at Jordan, particularly the enhanced soil carbon or evaporite influence during lowstands that may result in the pronounced  $\delta^{13}\text{C}$  minima (Allen and Matthews 1982, Immenhauser et al. 2008), although it appears likely that this overprint simply amplifies a primary global signal. Interestingly, a Maastriichtian  $\delta^{13}\text{C}_{\text{carb}}$  record from Zumaia also reveals two major negative shifts that are possibly linked to sea level fall, and interpreted to reflect cyclic variations on a  $\sim 1.2$  Myr scale (Batenburg et al. 2012).

Our findings are comparable to results obtained for the Oligocene (Lourens and Hilgen 1997, Pälike et al. 2006). There, 3<sup>rd</sup>-order sea-level minima are interpreted to occur at the nodes of a  $\sim 1.2$  Myr modulation of the obliquity cycle. Obliquity has its main impact on polar-latitude climates. Prolonged absence of summer melting during obliquity nodes results in higher accumulation of ice, which has been proposed as the cause of 3<sup>rd</sup>-order major regressions. Similarly, our results may indicate a mechanism that synchronizes sea-level and the global carbon cycle on a million-year time scale, during the mid-Cenomanian through mid-Turonian greenhouse time. The hypothesized climatic response to changes in Earth's obliquity is an obvious candidate for this million-year-scale oscillation, but explicit confirmation awaits additional appropriate high-resolution data series for which a continuous assessment of obliquity amplitude modulation can also be conducted. If the  $\sim 1.2$  Myr signal observed at Jordan is associated with this obliquity amplitude variation, then it is due to the interaction s3-s4 (Laskar et al. 2004), or the beat frequency between the orbital inclination variations of Earth(s3) and

Mars (s4). Cyclic climate-driven sea-level fluctuation consequently requires a long-period ( $10^5$  to  $10^6$  Myr) sustained alternation in the distribution of water between the oceans and the two equally potential, but controversial, continental fresh-water reservoirs of polar ice and/or aquifers (Hay and Leslie 1990, Jacobs and Sahagian 1993, 1995, Huber 1998, Huber et al. 2002, Miller et al. 2005, Bornemann et al. 2008, Francis et al. 2008, Miller et al. 2008, Föllmi 2013, MacLeod et al. 2013).

## 5. Conclusions

In conclusion, updated radioisotopic constraints and astrochronologic testing reveal an  $\sim 1$  Myr long oscillation associated with 3<sup>rd</sup>-order sea-level fluctuations on the Levant Platform. This cyclicity likely reflects a long-period obliquity ( $\sim 1.2$  Myr) control. 4<sup>th</sup>-order sea level cycles on the Levant Platform are interpreted to be linked to the  $\sim 400$  kyr-eccentricity cycle, and 5<sup>th</sup>-order depositional cycles are interpreted to be linked to the  $\sim 100$  kyr-eccentricity cycle. Being a global driver, eustasy and the global carbon cycle provide a mechanism for such astronomical control of stratigraphic sequence development, well documented in the Cenozoic, for which we present new evidence in the Mesozoic greenhouse. If this inference of astronomical forcing/pacing can be reproduced at other sites globally, it implies an important advance in resolving sequence stratigraphic discrepancies and ambiguities in geological dating, and it facilitates the global correlation of sequence boundaries.

**Acknowledgements.** This research was funded by the DFG grants KU 642/B20-1 and WE 4587/1-1 (Wendler), and US NSF grant EAR-0959108 (Meyers). We thank A. Masri (NRA, Jordan), R. Stein (AWI Bremerhaven), and M. Segl (Bremen University) for technical assistance. We are grateful to L. Hinnov (Johns Hopkins University), G. Weedon (Met Office Wallingford) and B. Huber (Smithsonian Institution) for comments on an earlier version of the manuscript. B. Sageman (Northwestern University) and M. Arthur (Pennsylvania State University) provided  $\delta^{13}\text{C}$  data from the U.S.G.S. #1 Portland core.

## References

- Allen, J. R., Matthews, R. K., 1982. Isotope signatures associated with early meteoric diagenesis. *Sedimentology* **29**, 797–817.
- Batenburg, S. J., Sprovieri, M., Gale, A. S., Hilgen, F. J., Hüsing, S., Laskar, J., Liebrand, D., Lirer, F., Orue-Etxebarria, X., Pelosi, N., Smit, J., 2012. Cyclostratigraphy



- and astronomical tuning of the Late Maastrichtian at Zumaia (Basque country, Northern Spain). *Earth and Planetary Science Letters* **359–360**, 264–278.
- Berger, A., Loutre, M., Laskar, J., 1992. Stability of the astronomical frequencies over the Earth's history for paleoclimate studies. *Science* **255**, 560–566.
- Bornemann, A., Norris, R.D., Friedrich, O., Beckmann, B., Schouten, S., Sinninghe Damsté, J.S., Vogel, J., Hoffmann, P., Wagner, T., 2008. Isotopic Evidence for Glaciation during the Cretaceous Supergreenhouse. *Science* **319**, 189–192.
- Bosence, D., Procter, E., Aurell, M., Bel Kahla, A., Boudagher-Fadel, M., Casaglia, F., Cirilli, S., Mehdie, M., Nieto, L., Rey, J., Scherreiks, R., Soussi, M., Waltham, D., 2009. A Dominant Tectonic Signal in High-Frequency, Peritidal Carbonate Cycles? A Regional Analysis of Liassic Platforms from Western Tethys. *Journal of Sedimentary Research* **79**, 389–415.
- Boullila, S., Galbrun, B., Miller, K.G., Pekar, S.F., Browning, J.V., Laskar, J., Wright, J.D., 2011. On the origin of Cenozoic and Mesozoic “third-order” eustatic sequences. *Earth-Science Reviews* **109**, 94–112.
- Elrick, M., Molina-Garza, R., Duncan, R., Snow, L., 2009. C-isotope stratigraphy and paleoenvironmental changes across OAE2 (mid-Cretaceous) from shallow-water platform carbonates of southern Mexico. *Earth and Planetary Science Letters* **277**, 295–306.
- Föllmi, 2013. Early Cretaceous life, climate and anoxia. *Cretaceous Research* **35**, 230–257.
- Francis, J.E., Ashworth, A., Cantrill, D.J., Crame, J.A., Howe, J., Stephens, R., Tosolini, A.-M., Thorn, V., 2008. 100 Million years of Antarctic climate evolution: Evidence from fossil plants. In: Cooper, A.K., Barrett, P.J., Stagg, H., Storey, B., Stump, E., Wise, W. and the 10th ISAES editorial team (Eds.), *Antarctica: A keystone in a changing world*. The National Academy Press, Washington, D.C., p. 19–28.
- Gale, A.S., Hardenbol, J., Hathway, B., Kennedy, W.J., Young, J.R., Phansalkar, V., 2002. Global correlation of Cenomanian (Upper Cretaceous) sequences; evidence for Milankovitch control on sea level. *Geology* **30**, 291–294.
- Gale, A.S., Young, J.R., Shackleton, N.J., Crowhurst, S.J., Wray, D.S., 1999. Orbital tuning of Cenomanian marly chalk successions; towards a Milankovitch time-scale for the Late Cretaceous. *Philosophical Transactions of the Royal Society A* **357**, 1815–1829.
- Gradstein, F.M., Gradstein, F.M., Ogg, J.G., Smith, A., Gradstein, F.M., Ogg, J.G., Smith, A., 2004. *A geologic time-scale*. Cambridge University Press, Cambridge, 610 pp.
- Gradstein, F.M., Ogg, J.G., Schmitz, M.D., Ogg, G.M., 2012. *The geologic time scale 2012*, First ed. Elsevier, Amsterdam, 1176 pp.
- Haq, B., U., Hardenbol, J., Vail, P.R., 1987. Chronology of fluctuating sea levels since the Triassic. *Science* **235**, 1156–1167.
- Haq, B.U., Al-Qahtani, A.M., 2005. Phanerozoic cycles of sea-level change on the Arabian Platform. *Geo Arabia* **10**, 127–160.
- Hardenbol, J., Thierry, J., Farlay, M.B., Jacquin, T., De Graciansky, P.-C.D., Vail, P.R., 1998. Mesozoic and Cenozoic sequence chronostratigraphic framework of European basins, Cretaceous biochronostratigraphy. In: De Graciansky, P.C., Hardenbol, J., Jacquin, T., Vail, P.R. (Eds.), *Mesozoic and Cenozoic sequence stratigraphy of European basins*. SEPM Special Publications **60**, p. 329–332.
- Hay, W.W., Leslie, M.A., 1990. Could possible changes in global groundwater reservoir cause eustatic sea level fluctuations? In: Geophysics Study Committee, C.o.P.S., Mathematics and Resources, National Research Council (Ed.), *Sea level change: Studies in geophysics*. The National Academy of Sciences, National Academy Press, Washington D.C., p. 161–170.
- Herbert, T.D., 1999. Towards a composite orbital chronology for the Late Cretaceous and Early Palaeocene GPTS. *Philosophical Transactions of the Royal Society A* **357**, 1891–1905.
- Huber, B.T., 1998. Perspectives – Paleoclimate – Tropical paradise at the Cretaceous poles? *Science* **282**, 2199–2200.
- Huber, B.T., Norris, R.D., MacLeod, K.G., 2002. Deep-sea paleotemperature record of extreme warmth during the Cretaceous. *Geology* **30**, 123–126.
- Immenhauser, A., Holmden, C., Patterson, W.P., 2008. Interpreting the carbon isotope record of ancient epeiric seas: lessons from the Recent. *Geological Association of Canada Special Publication* **48**, 135–174.
- Jacobs, D.K., Sahagian, D.L., 1993. Climate-induced fluctuations in sea level during non-glacial times. *Nature* **361**, 710–712.
- Jacobs, D.K., Sahagian, D.L., 1995. Milankovitch fluctuations in sea level and recent trends in sea-level change: Ice may not always be the answer. In: Haq, B.U. (Ed.), *Sequence Stratigraphy and Depositional Response to Eustatic, Tectonic and Climatic Forcing*, p. 329–366.
- Jarvis, I., Gale, A., Jenkyns, H.C., Pearce, M.A., 2006. Secular variation in Late Cretaceous carbon isotopes: a new  $\delta^{13}\text{C}$  carbonate reference curve for the Cenomanian-Campanian (99.6–70.6 Ma). *Geological Magazine* **143**, 561–608.
- Knauth, L.P., Kennedy, M.J., 2009. The late Precambrian greening of the Earth. *Nature* **460**, 728–732.
- Kuhnt, W., Holbourn, A., Gale, A., Chellai, E., Kennedy, W.J., 2009. Cenomanian sequence stratigraphy and sea-level fluctuations in the Tarfaya Basin (SW Morocco). *Geological Society of America Bulletin* **121**, 1695–1710.
- Laskar, J., Fienga, M., Gastineau, M., Manche, H., 2011. La2010: a new orbital solution for the long-term motion of the Earth. *Astronomy and Astrophysics* **532**, A89, 81–15.
- Laskar, J., Robutel, P., Joutel, F., Gastineau, M., Correia, A.C.M., Levrard, B., 2004. A long-term numerical solution for the insolation quantities of the Earth. *Astronomy and Astrophysics* **428**, 261–285.
- Lourens, L.J., Hilgen, F.J., 1997. Long-periodic variations in the Earth's obliquity and their relation to third-order eustatic cycles and late Neogene glaciations. In: Part-

- ridge, T. C. (Ed.), *The Plio-Pleistocene boundary*. Pergamon, Oxford, United Kingdom, p. 43–52.
- MacLeod, K. G., Huber Brian, T., Jiménez Berrocoso, Á., Wendler, I., 2013. A stable and hot Turonian without glacial  $\delta^{18}\text{O}$  excursions is indicated by exquisitely preserved Tanzanian foraminifera. *Geology* **41**, 1083–1086.
- Mathews, R. K., Frohlich, C., 2002. Maximum flooding surfaces and sequence boundaries: comparisons between observations and orbital forcing in the Cretaceous and Jurassic (65–190 Ma). *Geo Arabia* **7**, 503–538.
- Meyers, S. R., 2012. Seeing red in cyclic stratigraphy: Spectral noise estimation for astrochronology. *Paleoceanography* **27**, PA3228.
- Meyers, S. R., Hinnov, L. A., 2010. Northern Hemisphere glaciation and the evolution of Plio-Pleistocene climate noise. *Paleoceanography* **25**, doi:10.1029/2009PA001834
- Meyers, S. R., Sageman, B. B., 2007. Quantification of deep-time orbital forcing by average spectral misfit. *American Journal of Science* **307**, 773–792.
- Meyers, S. R., Sageman, B. B., Arthur M. A., 2012a. Obliquity forcing of organic matter accumulation during Oceanic Anoxic Event 2. *Paleoceanography* **27**, PA3212.
- Meyers, S. R., Sageman, B. B., Hinnov, L. A., 2001. Integrated quantitative stratigraphy of the Cenomanian-Turonian Bridge Creek Limestone Member using evolutive harmonic analysis and stratigraphic modeling. *Journal of Sedimentary Research* **71**, 628–644.
- Meyers, S. R., Siewert, S. E., Singer, B. S., Sageman, B. B., Condon, D. J., Obradovich, J. D., Jicha, B. R., Sawyer, D. A., 2012b. Intercalibration of radioisotopic and astrochronologic time scales for the Cenomanian-Turonian boundary interval, Western Interior Basin, USA. *Geology* **40**, 7–10.
- Miller, K. G., Kominz, M. A., Browning, J. V., Wright, J. D., Mountain, G. S., Katz, M. E., Sugarman, P. J., Cramer, B. S., Christie-Blick, N., Pekar, S. F., 2005. The Phanerozoic Record of Global Sea-Level Change. *Science* **310**, 1293–1298.
- Miller, K. G., Wright, J. D., Katz, M. E., Browning, J. V., Cramer, B. S., Wade, B. S., Mizintseva, S. F., 2008. A view of Antarctic ice-sheet evolution from sea-level and deep-sea isotope changes during the Late Cretaceous–Cenozoic. In: Cooper, A. K., Barrett, P. J., Stagg, H., Storey, B., Stump, E., Wise, W. and the 10th ISAES editorial team (Eds.), *Antarctica: A keystone in a changing world*. The National Academy Press, Washington, D. C., p. 55–70.
- Morsi, A.-M. M., Wendler, J. E., 2010. Biostratigraphy, palaeoecology and palaeogeography of the Middle Cenomanian–Early Turonian Levant Platform in Central Jordan based on ostracods. *Geological Society of London Special Publication* **341**, 187–210.
- Pälike, H., Norris, R. D., Herrle, J. O., Wilson, P. A., Coxall, H. K., Lear, C. H., Shackleton, N. J., Tripathi, A. K., Wade, B. S., 2006. The heartbeat of the Oligocene climate system. *Science* **314**, 1894–1898.
- Peryt, T. M., Scholle, P. A., 1996. Regional setting and role of meteoric water in dolomite formation and diagenesis in an evaporite basin: studies in the Zechstein (Permian) deposits of Poland. *Sedimentology* **43**, 1005–1023.
- Powell, J. H., 1988. The geology of Karak. *Bulletin Geology Directorate, Natural Resources Authority (Ministry of Energy and Mineral Resources) Amman* **8**, Map Sheet No. 3152/III.
- Powell, J. H., 1989. Stratigraphy and sedimentation of the Phanerozoic rocks in central and southern Jordan. *Bulletin Geology Directorate, Natural Resources Authority (Ministry of Energy and Mineral Resources) Amman* **11**, 161 pp.
- Powell, J. H., Mohammed, B. K., 2011. Evolution of Cretaceous to Eocene alluvial and carbonate platform sequences in central and south Jordan. *Geo Arabia* **16**, 29–82.
- Robaszynski, F., Gale, A., Juignet, P., Amedro, F., Hardenbol, J., 1998. Sequence stratigraphy in the Upper Cretaceous series of the Anglo-Paris Basin; exemplified by the Cenomanian Stage. In: de Graciansky Pierre, C., Hardenbol, J., Jacquin, T., Vail Peter, R. (Eds.), *Mesozoic and Cenozoic sequence stratigraphy of European basins*. SEPM Special Publications **60**, 363–386.
- Sageman, B. B., Meyers, S. R., Arthur, M. A., 2006. Orbital timescale and new C-isotope record for Cenomanian–Turonian boundary stratotype. *Geology* **34**, 125–128.
- Schulze, F., Lewy, Z., Kuss, J., Gharaibeh, A., 2003. Cenomanian–Turonian carbonate platform deposits in west central Jordan. *International Journal of Earth Sciences* **92**, 641–660.
- Schulze, F., Marzouk, A. M., Bassiouni, M. A. A., Kuss, J., 2004. The late Albanian–Turonian carbonate platform succession of west-central Jordan: stratigraphy and crises. *Cretaceous Research* **25**, 709–737.
- Sepúlveda, J., Wendler, J., Leider, A., Kuss, J., Summons, R. E., Hinrichs, K.-U., 2009. Molecular-isotopic evidence of environmental and ecological changes across the Cenomanian–Turonian boundary in the Levant Platform of central Jordan. *Organic Geochemistry* **40**, 553–568.
- Sharland, P. R., Casey, D. M., Davies, R. B., Simmons, M., Sutcliffe, O. E., 2004. Arabian plate sequence stratigraphy – revisions to SP2. *Geo Arabia* **9**, 199–214.
- Simmons, M. D., Sharland, P. R., Casey, D. M., Davies, R. B., Sutcliffe, O. E., 2007. Arabian Plate sequence stratigraphy: Potential implications for global chronostratigraphy. *GeoArabia* **12**, 101–130.
- Sprovieri, M., Coccioni, R., Lirer, F., Pelosi, N., Lozar, F., 2006. Orbital tuning of a lower Cretaceous composite record (Maiolica Formation, central Italy). *Paleoceanography* **21**, PA4212.
- Sprovieri, M., Sabatino, N., Pelosi, N., Batenburg, S. J., Coccioni, R., Iavarone, M., Mazzola, S., 2013. Late Cretaceous orbitally-paced carbon isotope stratigraphy from the Bottacione Gorge (Italy). *Paleogeography Palaeoclimatology Palaeoecology* **279–380**, 81–94.
- Strasser, A., Hillgärtner, H., Hug, W., Pittet, B., 2000. Third-order depositional sequences reflecting Milankovitch cyclicity. *Terra Nova* **12**, 303–311.
- Thomson, D. J., 1982. Spectrum Estimation and harmonic analysis. *Proceedings of the IEEE* **70**, 1055–1096.
- Thomson, D. J., Lanzerotti, L. J., MacLennan, C. G., 2001. The interplanetary magnetic field: Statistical properties

- and discrete modes. *Journal of Geophysical Research* **106**, 15941–15962.
- Vaughan, S., Bailey, R., Smith, D. G., 2011, Detecting cycles in stratigraphic data: Spectral analysis in the presence of red noise. *Paleoceanography* **26**, PA4211, doi:10.1029/2011PA002195
- Voigt, S., Erbacher, J., Mutterlose, J., Weiss, W., Westerhold, T., Wiese, F., Wilmsen, M., Wonik, T., 2008. The Cenomanian-Turonian of the Wunstorf section (North Germany): global stratigraphic reference section and new orbital time scale for Oceanic Anoxic Event 2. *Newsletters on Stratigraphy* **43**, 65–89.
- Voigt, S., Gale, A. S., Voigt, T., 2006. Sea-level change, carbon cycling and palaeoclimate during the Late Cenomanian of northwest Europe; an integrated palaeoenvironmental analysis. *Cretaceous Research* **27**, 836–858.
- Wade, B. S., Pälike, H., 2004. Oligocene climate dynamics. *Paleoceanography* **19**, 1–16.
- Wendler, I., Wendler, J., Neuhuber, S., Wägrich, M., 2009. Productivity fluctuations and orbital cyclicity during onset of Early to Middle Turonian marine red-bed formation (Austrian Eastern Alps). *SEPM Special Publications* **91**, 209–221.
- Wendler, I., 2013. A critical evaluation of carbon isotope stratigraphy and biostratigraphic implications for Late Cretaceous global correlation. *Earth-Science Reviews* **126**, 116–146.
- Wendler, J. E., Wendler, I., Kuss, H. J., 2009. Early Turonian shallow marine red beds on the Levant carbonate platform (Jordan), Southern Tethys. *SEPM Special Publications* **91**, 179–187.
- Wendler, J. E., Lehmann, J., Kuss, J., 2010. Orbital time scale, intra-platform basin correlation, carbon isotope stratigraphy, and sea level history of the Cenomanian/Turonian Eastern Levant platform, Jordan. *Geological Society of London Special Publication* **341**, 171–186.
- Wiese, F., Schulze, F., 2005. The upper Cenomanian (Cretaceous) ammonite *Neolobites vibrayanus* (d'Orbigny, 1841) in the Middle East: taxonomic and palaeoecologic remarks. *Cretaceous Research* **26**, 930–946.
- Wilkinson, B. H., Diedrich, N. W., Drummond, C. N., 1996. Facies successions in peritidal carbonate sequences. *Journal of Sedimentary Research* **66**, 1065–1078.
- Wilkinson, B. H., Drummond, C. N., Diedrich, N. W., Rothman, E. D., 1999. Poisson processes of carbonate accumulation on Paleozoic and Holocene platforms. *Journal of Sedimentary Research* **69**, 338–350.
- Wilmsen, M., 2003. Sequence stratigraphy and palaeoceanography of the Cenomanian Stage in northern Germany. *Cretaceous Research* **24**, 525–568.
- Wilmsen, M., Niebuhr, B., Hiss, M., 2005. The Cenomanian of northern Germany: facies analysis of a transgressive biosedimentary system. *Facies* **51**, 242–263.

Manuscript received: October 11, 2013; rev. version accepted: October 14, 2013.